IEEE Sensors Council

Height Estimation for Floor Identification in Elevator and Escalator Scenarios Based on Smartphones Built-in IMU

Shiyi Chen, Jian Kuang, Dazhou Xia, Xiaoji Niu

***Abstract*—Accurate floor identification within multi-story buildings is crucial for guiding pedestrians to their destinations in complex door environments like shopping centers, airports and office buildings. Current floor identification methods primarily rely on barometers or wireless signals, which are susceptible to environmental influences or require extensive maintenance. This paper proposes an innovative method for floor identification by estimating pedestrian height using the built-in inertial measurement unit (IMU) of smartphones. By analyzing pedestrian motion in elevator and escalator scenarios, distinct pedestrian motion constraints are derived. An inertial navigation system (INS) framework is employed, which utilizes an extended Kalman Filter (EKF) to integrate these constraints and estimate height changes as pedestrians transition between floors. The method includes detailed motion modeling, taking into account the distinct patterns in elevators and escalators. The proposed algorithm is validated through multiple experiments in a typical shopping mall, demonstrating significant accuracy enhancements with relative height errors of 2.98% (up) and 1.45% (down) in elevator scenarios, and 3.50% (up) and 7.97% (down) in escalator scenarios. This indicates a substantial improvement over existing techniques. Notably, the method does not rely on barometric sensors or prior signal fingerprint databases, highlighting its potential universality across common mobile devices.**
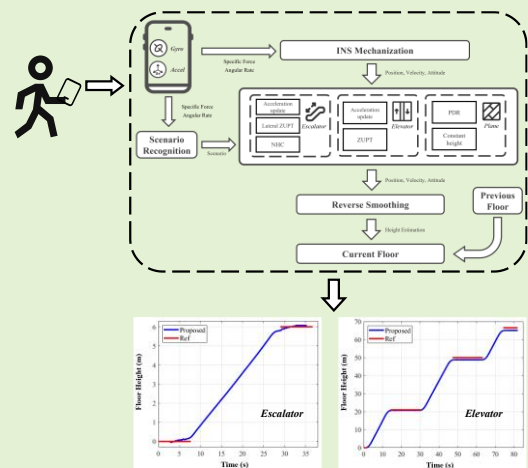
***Index Terms*—Indoor Positioning, Floor Identification, Smartphone, IMU, Pedestrian Motion Constraint.**

I. Introduction

Reliable and precise positioning is the guarantee of Location-Based Services (LBS)[1], [2]. In indoor environments, identifying the specific floor where pedestrians are located is crucial for achieving accurate indoor positioning[3], [4]. In emergency rescue scenarios, such as fires and natural disasters, precise floor information can significantly expedite rescue efforts[5], [6]. Consequently, indoor positioning systems must provide both horizontal and vertical location information (floor information). This capability is vital for enhancing safety, commercial value, and user satisfaction. Meanwhile, given the widespread use of smartphones and the multitude of built-in sensors, current pedestrian positioning methods based on smartphones can also be extended to include floor identification[7].

Nowadays, extensive research has been conducted on methods for floor identification in indoor positioning, which

Shiyi Chen and Dazhou Xia are with the School of Geodesy and Geomatics, Wuhan University, Wuhan 430079, China (e-mail: chenshiyi@whu.edu.cn; dzhxia@whu.edu.cn).
Jian Kuang is with the GNSS Research Center, Wuhan University, Wuhan 430079, China (e-mail: kuang@whu.edu.cn).
Xiaoji Niu is with the GNSS Research Center, Wuhan University, Wuhan, Hubei 430079, China, and also with the Hubei Luojia Labor- -atory, Wuhan, Hubei 430079, China (e-mail: xjniu@whu.edu.cn)

can be classified into two categories based on their reliance on prior information: fingerprint matching based methods and height estimation based methods. Among these, Wi-Fi, cellular networks, and magnetic fields are commonly used signals for fingerprint matching schemes. Barometers and IMUs are typical sensors for height measurement schemes.

Inertial sensors are capable of detecting acceleration changes in a pedestrian's upward and downward motion. By integrating the vertical acceleration over time, it is possible to calculate changes in vertical velocity and subsequently changes in vertical position (i.e. displacement), which can be used to identify floors. For pedestrians, the main scenarios for floor transitions include stairs, elevators and escalators. In stair scenarios, pedestrian movement characteristics are relatively abundant, making it easier to obtain vertical velocity. However, there are fewer pedestrian movement characteristics in elevator and escalator scenarios. Thus, height estimation using inertial sensors in these two scenarios is challenging.

For pedestrian height estimation using inertial sensors, the essential problem is the rapid drift of the INS positioning due to low-grade sensors. The key solution is to mitigate such drift, especially in the vertical direction. In this paper, we explore the feasibility of utilizing inertial sensors in smartphones to analyze pedestrian motion characteristics in elevator and escalator scenarios. For pedestrians, it is typically assumed that they access a building from the first floor. Floor identification is achievable by estimating the height change from the initial point to the current position.

This study proposes a pedestrian floor identification

method based on inertial sensors in smartphones, offering a solution for pedestrian height estimation in elevator and escalator scenarios. We assume the starting floor of the pedestrian is known, and estimating height variations enables the identification of subsequent floors. We derive distinct pedestrian motion constraints by analyzing the pedestrian motion in these two scenarios. Then, we employ the INS framework, integrating the pedestrian motion constraint information using the Extended Kalman Filter (EKF). This solution employs only inertial sensors and pedestrian motion characteristics, ensuring it is self-contained, robust, and reliable.

The remaining parts of this paper is organized as follows. Section II summarizes related previous works. Section III describes characteristic analysis in elevator and escalator scenarios. Section IV presents the system algorithm framework and corresponding methods. Section V discusses the experimental setting and results. Finally, the conclusion and outlook are provided in Section VI.

II. Related Work

In this section, we summarize the previous related work on floor identification. Based on whether prior information is required, current work can be divided into two categories: fingerprint matching based method and height estimation based methods.

A. Fingerprint matching based Methods

Fingerprint matching based floor identification methods primarily involve utilizing the difference in signal strength between different floors for floor identification[8]. Wi-Fi and cellular networks are popular wireless signals used for this purpose, as they are widely available in buildings and can provide information about the floor where a device is located. Fingerprint matching methods are primarily categorized into statistical-based and machine learning-based methods. Some researchers utilized statistical-based methods for floor identification, such as K-Means clustering[9], Linear Discriminant Analysis[10], Fisher's Linear Discriminant[11] and particle filtering[12]. Currently, with the advancement of artificial intelligence, machine learning-based methods have become the mainstream research direction in floor identification due to their high accuracy and robustness. Various machine learning models, such as K-Nearest Neighbors[13], Naive Bayes[14], clustering[15], Auto-Encoder[16],Multilayer Perceptron[17], convolutional neural networks[18], [19] and Long Short-Term Memory neural networks[20] have been explored for floor identification. Additionally, barometer and accelerometer measurements are integrated with wireless signals to assist in floor recognition. Ye utilized the accelerometer's capability to capture device motion patterns and changes, coupling it with Wi-Fi signals[21]. Models such as Bar-Fi[22], Hy-Rise[23], Zee-Fi[6] combine barometric measurements with Wi-Fi for floor identification.

Meanwhile, due to the temporal stability and spatial distinguishability of magnetic signals[24], the magnetic signals can also be used for floor identification. Zhao utilized the Euclidean closest approximation and majority principle to identify floor[25]. Ashraf used a naive Bayes classifier algorithm to determine user's activities, and then matched the magnetic field data with the magnetic field database to estimate floor[26].

Although these fingerprint matching methods offer higher precision in floor identification, they require large fingerprint databases and infrastructure deployment, entailing limitations and high maintenance costs.

B. Height Estimation based Methods

The floor identification methods based on height estimation primarily utilize height measurement sensors to track changes in user's height and infer the floor[27]. Barometers and inertial sensors are commonly employed for this purpose. Barometers gauge height changes by measuring atmospheric pressure variations, which decrease as elevation increases[3], [28]. Several studies have focused on using barometers to measure height variation for floor identification. Shin compensated for barometers bias by sea-level pressure and calculated elevation information by barometric height conversion formula[29]. Zhao assumed atmospheric parameters and converted the measured atmospheric pressure to height using the barometric equation[30]. However, the accuracy of height estimation is influenced by environmental factors such as temperature and humidity[31]. Additionally, in this paper, we conducted a survey of the built-in sensors in common smartphones during recent years, including Apple, Huawei, Samsung, Xiaomi and other major brands, totaling 100 smartphone models. Survey suggested that only 34 of these smartphones have built-in barometers. For most of smartphones without barometers, the height estimation methods based on barometers still cannot address the requirements of floor identification.

Devices used for height estimation with inertial sensors include mobile phones and wearable inertial modules. Ye proposed F-Track, which leverages a mobile phone's accelerometer to identify the pedestrian's current floor levels by mapping traveling time in elevators or step counts on stairs to floor levels[32]. Li introduced a moving platform correction model to achieve position tracking during rides on elevators or escalators based on inertial sensor modules[33]. Most research on floor identification using inertial sensors focuses on scenarios involving pedestrians traversing stairs[13], [34], where distinct movement characteristics facilitate height estimation through motion pattern analysis. Wearable inertial modules, being stably fixed, offer more easily distinguishable characteristics; hence, most current research in this area is based on such platforms[35], [36], [37]. However, wearable inertial modules require users to wear additional devices, which can impact user adoption and comfort, especially when worn for prolonged durations. Consequently, these devices are not widely used as a daily platform for pedestrian floor identification.

III. Scenario Characteristic Analysis

In this section, we analyze the characteristics of two scenarios: elevator and escalator, along with the movement patterns of pedestrians in these two scenarios. Elevator and escalator scenarios are narrow typically. As pedestrians take elevators and escalators, the motion tends to be relatively constrained, resulting in a relatively stable state of motion. The movement of pedestrians is inherently linked to the operation of the elevator and escalator.

A. Elevator Scenario

The operation of elevators can be categorized into multi-floor and single-floor transit operation modes, with similar characteristics but slight difference. Prior to the elevator's

movement and subsequent to its cessation, there is typically a short static period when the cab door open/close. Due to the narrow space inside the elevator cabs, pedestrians tend to stand still during this short static period, with their phones considered zero velocity.

$$\tilde{\boldsymbol{v}}^n = \begin{bmatrix} 0 & 0 & 0 \end{bmatrix}^T \quad (1)$$

where $\tilde{\boldsymbol{v}}^n$ is the velocity of the smartphone, superscript "n" refers to the navigation frame (n-frame).

Meanwhile, for the multi-floor transit operation mode, the elevator cab will sustain a constant speed of ascent or descent for an extended duration in the middle of the movement. During this period, it can be assumed that pedestrians are not experiencing external acceleration. In this state, the specific force read by the inertial sensor is primarily attributable to the Earth's gravity acceleration.

$$\boldsymbol{f}^n = -\boldsymbol{g}^T = \begin{bmatrix} 0 & 0 & -g \end{bmatrix}^T \quad (2)$$

where $\boldsymbol{f}^n$ is the specific force in the n-frame. g is the gravity of the Earth.

On the contrary, for the single-floor transit operation mode, the elevator cab will decelerate right after accelerate without any constant speed period. Figure. 1 shows the phone acceleration norm in the single-floor (from 16th to 17th floor) and the multi-floor (from 1st to 17th floor) operation mode respectively, while pedestrians hold the smartphones during elevator transit.
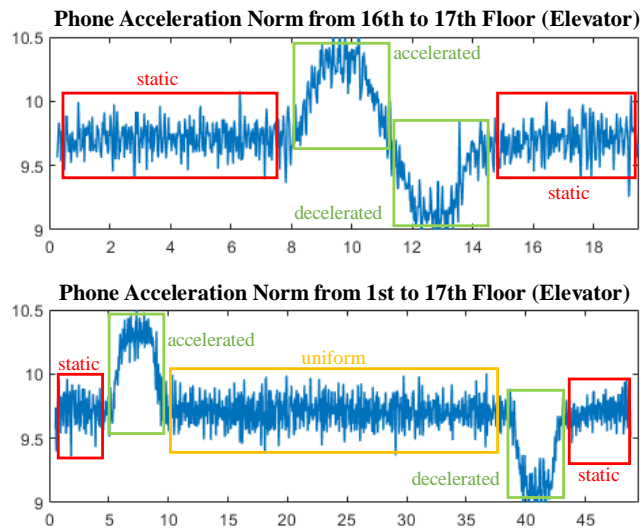

Phone Acceleration Norm from 16th to 17th Floor (Elevator)

Phone Acceleration Norm from 1st to 17th Floor (Elevator)

Fig. 1. The change in phone acceleration norm while pedestrians take the elevator.

B. Escalator Scenario

When pedestrians take escalators, the confined nature of the escalator dictates that pedestrians move at a constant speed along with the escalator. Pedestrians exhibit forward and vertical velocity, while their lateral velocity is zero. Therefore, in this case, pedestrians demonstrate motion characteristics as depicted in formula (2). Typically, pedestrians hold smartphones ahead while going to escalators. During this time, the impact of the misalignment angle between the smartphone's heading and the walking direction can be disregarded. It can be assumed that the orientation of the pedestrian aligns with the direction of the escalator. Thus, in the smartphone's coordinate system, the lateral velocity is zero.

$$v_{lateral}^b = 0 \quad (3)$$

where $v_{lateral}^b$ is the lateral velocity of the smartphone, superscript "b" is the body frame (b-frame).

Different with the elevator scenarios, pedestrians in escalator scenarios do not experience a state of zero velocity. Correspondingly, prior to stepping onto and after stepping off the escalator, pedestrians only have forward velocity, with lateral and vertical velocity as zero. For the smartphone holding ahead, both lateral and vertical velocity are zero in the b-frame

$$\boldsymbol{v}^b = \begin{bmatrix} v_{PDR} & 0 & 0 \end{bmatrix}^T \quad (4)$$

where $\boldsymbol{v}^b$ is the velocity of the smartphone in the b-frame, v_{PDR} is the estimated forward velocity. In this case, pedestrians' forward speed v_{PDR} is mainly determined by the step detection and step length estimation algorithm. In this paper, we apply the conventional peak detection algorithm to detect steps, while the step length estimation algorithm employs the linear model[38]. Figure. 2 shows the phone acceleration norm during the escalator transit from the 1st to 2nd floor when pedestrians hold smartphones ahead.

Phone Acceleration Norm from 1st to 2nd Floor (Escalator)
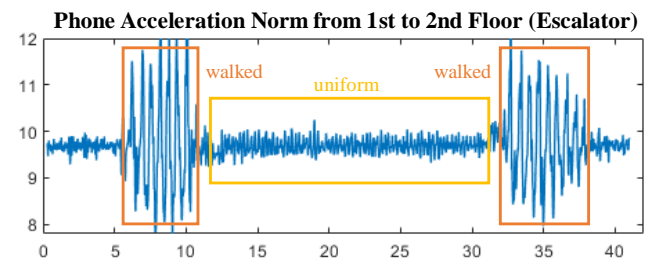
Fig. 2. The change in phone acceleration norm while pedestrians take the escalator.

The pedestrian motion characteristics in both elevator and escalator scenarios can be employed as constraint information, serving to limit the growth of errors within INS. These motion constraints prove crucial in suppressing the divergence of navigation solutions due to the accumulation of INS errors. Based on these constraints, we can establish motion constraint equations. A comprehensive exposition of these equations will be presented in Section IV.

IV. Algorithm Design

The system algorithm framework for the proposed pedestrian floor identification method is depicted in Figure. 3. We employ the inertial mechanization as the foundational framework and categorize scenarios into elevator, escalator, and plane. In this paper, we used manual calibration for scenario recognition. While there have been some relatively mature solutions for scenario recognition, such as spatial landmark[39], the focus of this paper lies on the height estimation and floor identification of pedestrians in elevator and escalator scenarios. Thus, we do not conduct relevant research on scenario recognition.

After distinguishing the scenarios, according to the scenario analysis in Section III, pedestrian motion constraint observations can be obtained for each scenario. In elevator scenarios, zero velocity update (ZUPT)[40] and acceleration update, as shown in formula (1) and (2) are used to mitigate the accumulation errors. In escalator scenarios, we employ acceleration update, zero lateral velocity update (Lateral ZUPT) and non-holonomic constraint (NHC)[41] methods, as shown by formula (2)(3)(4). We also separately distinguish the plane scenario from elevators and escalators. In plane scenarios, we use height locking to mitigate the
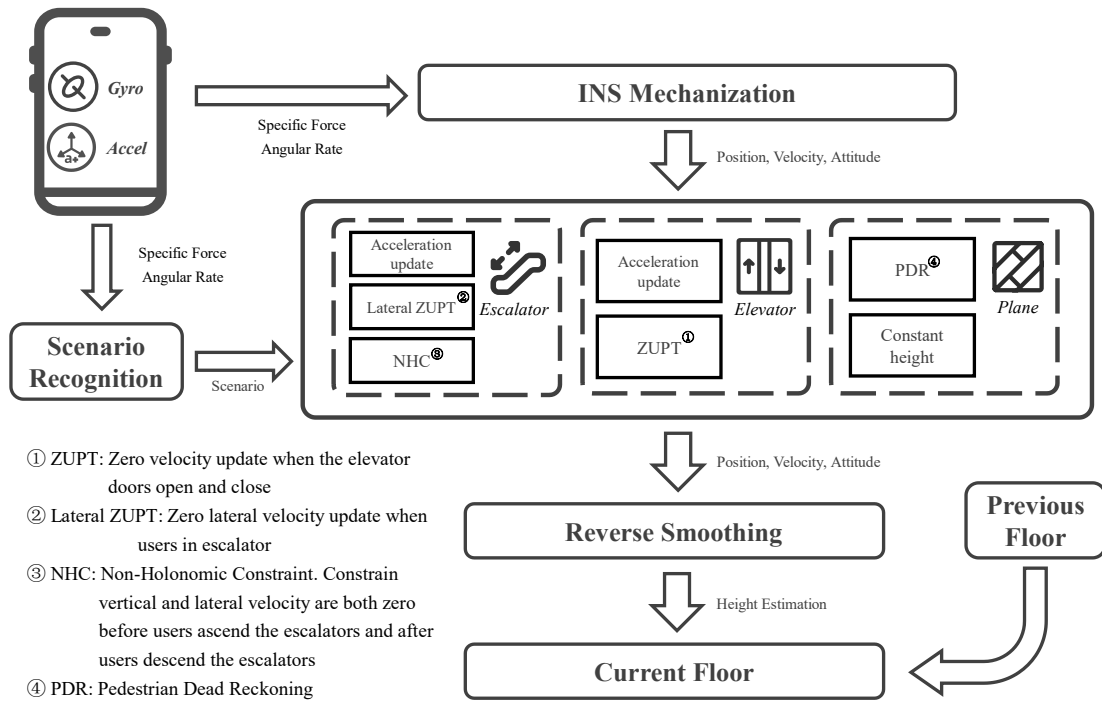
Fig. 3. Pedestrian Floor Identification System Algorithm Framework

height divergence of PDR.

Inertial mechanization integrates the acceleration and angular velocity output from the IMU to estimate the pedestrian's height changes. By utilizing the pedestrian motion constraints in these scenarios, we suppress error divergence to achieve more accurate height estimation. Meanwhile, the reverse smoothing algorithm is employed to enhance system stability[42]. The following will introduce each part of the algorithm in detail.

A. INS Mechanization

The fundamental principle of INS mechanization is to calculate the user's position, velocity and attitude at the next time based on the known position, velocity and attitude at the current time through the angular velocity and specific force output by gyroscopes and accelerometers. However, due to the substantial noise levels in the built-in IMU of the smart-phone, correcting minor error terms is ineffectual in enhancing navigation performance. Therefore, in this paper, we disregard the impact of the Earth's rotational angular velocity and the angular velocity of entrainment caused by pedestrian motion and velocity sculling effect. Simplified INS mechanization can be written as

$$\begin{bmatrix} \boldsymbol{p}_k^n \\ \boldsymbol{v}_k^n \\ \boldsymbol{C}_{b,k}^n \end{bmatrix} = \begin{bmatrix} \boldsymbol{p}_{k-1}^n + \boldsymbol{D}_R^{-1} \boldsymbol{v}_{k-1/2}^n \Delta t_k \\ \boldsymbol{v}_{k-1}^n + \boldsymbol{C}_{b,k}^n \left(\Delta \boldsymbol{v}_k^b + \dfrac{\Delta \boldsymbol{\theta}_k^b \times \Delta \boldsymbol{v}_k^b}{2} \right) - \boldsymbol{g}^n \Delta t_k \\ \boldsymbol{C}_{b,k-1}^n \left(\boldsymbol{I}_3 + \left(\Delta \boldsymbol{\theta}_k^b + \dfrac{\Delta \boldsymbol{\theta}_{k-1}^b \times \Delta \boldsymbol{\theta}_{k-1}^b}{12} \right) \times \right) \end{bmatrix} \quad (5)$$

$$\begin{cases} \boldsymbol{D} = \mathrm{diag}\left(\begin{bmatrix} R_m + h & (R_n + h)\cos B & -1 \end{bmatrix} \right) \\ \Delta \boldsymbol{\theta}_k^b = (\boldsymbol{\omega}_k^b - \boldsymbol{b}_{g,k}) \Delta t_k \\ \Delta \boldsymbol{v}_k^b = (\boldsymbol{f}_k^b - \boldsymbol{b}_{f,k}) \Delta t_k \end{cases}$$

where $\boldsymbol{p}^n$ and $\boldsymbol{v}^n$ are the position and velocity in the n-frame; $\boldsymbol{C}_b^n$ is the rotation matrix that denote the rotation of the b-frame with respect to the n-frame; R_m and R_n are the curvature radius of the meridian and the prime vertical, respectively; $\mathbf{g}^n$ is the gravity vector in the n-frame; $\boldsymbol{\omega}^b$

and $\boldsymbol{f}^b$ are the angular velocity and acceleration from the IMU, respectively; $\boldsymbol{b}_g$ and $\boldsymbol{b}_f$ are the bias of the gyroscope and accelerometer, respectively; $\boldsymbol{I}_3$ is the 3×3 identity matrix; Δt_k is time interval from the (k-1)-th epoch to the k-th epoch; $(\cdot) \times$ denotes the skew-symmetric matrix of the vector.

B. Filter Design

The Kalman Filter algorithm is one of the most common methods in data fusion. The algorithm estimates state more accurately by integrating various types of observations. In this paper, we employ the Extend Kalman Filter (EKF) to mitigate the negative effect of nonlinearization. The filter state is defined as the navigation error state.

The system state equation of the filter can be derived from the differentiation of the INS mechanization algorithm. This process can be referenced in paper[43]. The error state vector can be written as

$$\delta \boldsymbol{x} = \begin{bmatrix} (\delta \boldsymbol{p}^n)^T & (\delta \boldsymbol{v}^n)^T & \boldsymbol{\phi}^T & (\delta \boldsymbol{b}_g)^T & (\delta \boldsymbol{b}_a)^T \end{bmatrix}^T \quad (6)$$

where $\delta \boldsymbol{p}^n$, $\delta \boldsymbol{v}^n$ and $\boldsymbol{\phi}$ are the position error, velocity error and attitude error in the n-frame; $\delta \boldsymbol{b}_g$ and $\delta \boldsymbol{b}_a$ are the error of the gyroscope bias and accelerometer bias, respectively. Equation of state can be written as

$$\begin{cases} \delta \boldsymbol{x}_{k,k-1} = \Phi_{k,k-1} \delta \boldsymbol{x}_{k-1} \\ \boldsymbol{P}_{k,k-1} = \Phi_{k-1} \boldsymbol{P}_{k-1,k-1} \Phi_{k-1}^T + \boldsymbol{Q}_k \\ \boldsymbol{Q}_k \approx \dfrac{\Delta t}{2} \left[\Phi_{k,k-1} \boldsymbol{Q}(t_k) + \boldsymbol{Q}(t_k) \Phi_{k,k-1}^T \right] \end{cases} \quad (7)$$

where $\delta \boldsymbol{x}$ is the navigation error state vector; $\boldsymbol{P}$ is the covariance matrix of the navigation error state; $\boldsymbol{Q}$ is the noise matrix of system state. State transition matrix $\boldsymbol{\Phi}$ can be written as

① ZUPT: Zero velocity update when the elevator doors open and close
② Lateral ZUPT: Zero lateral velocity update when users in escalator
③ NHC: Non-Holonomic Constraint. Constrain vertical and lateral velocity are both zero before users ascend the escalators and after users descend the escalators
④ PDR: Pedestrian Dead Reckoning

$$\boldsymbol{\Phi}_{k,k-1} = \begin{bmatrix} \boldsymbol{I}_3 & \boldsymbol{I}_3 \Delta t_k & \boldsymbol{0} & \boldsymbol{0} & \boldsymbol{0} \\ \boldsymbol{0} & \boldsymbol{I}_3 & (\boldsymbol{f}_k^n \times) \Delta t_k & \boldsymbol{0} & \boldsymbol{C}_{b,k}^n \Delta t_k \\ \boldsymbol{0} & \boldsymbol{0} & \boldsymbol{I}_3 & -\boldsymbol{C}_{b,k}^n \Delta t_k & \boldsymbol{0} \\ \boldsymbol{0} & \boldsymbol{0} & \boldsymbol{0} & \boldsymbol{I}_3 \cdot exp\left(\frac{-\Delta t_k}{\tau}\right) & \boldsymbol{0} \\ \boldsymbol{0} & \boldsymbol{0} & \boldsymbol{0} & \boldsymbol{0} & \boldsymbol{I}_3 \cdot exp\left(\frac{-\Delta t_k}{\tau}\right) \end{bmatrix} \tag{8}$$

where τ is the correlation time of first order Markov Process. When observations are available, such as velocity of pedestrian, the measurement equation can be established, and it can be written as

$$\delta \boldsymbol{z}_k = \boldsymbol{H}_k \delta \boldsymbol{x}_{k,k-1} + \boldsymbol{n}_k \tag{9}$$

where $\delta \boldsymbol{z}$ is the difference between predictions and observations; $\boldsymbol{H}$ is the design matrix; $\boldsymbol{n}$ is the noise of the observations. Measurement update of the navigation error state and its covariance matrix can be written as

$$\begin{cases} \boldsymbol{K}_k = \boldsymbol{P}_{k,k-1} \boldsymbol{H}_k^T (\boldsymbol{H}_k \boldsymbol{P}_{k,k-1} \boldsymbol{H}_k^T + \boldsymbol{R}_k)^{-1} \\ \boldsymbol{x}_k = \boldsymbol{x}_{k,k-1} + \boldsymbol{K}_k (\delta \boldsymbol{z}_k - \boldsymbol{H}_k \boldsymbol{x}_{k,k-1}) \\ \boldsymbol{P}_k = (\boldsymbol{I} - \boldsymbol{K}_k \boldsymbol{H}_k) \boldsymbol{P}_{k,k-1} (\boldsymbol{I} - \boldsymbol{K}_k \boldsymbol{H}_k)^T + \boldsymbol{K}_k \boldsymbol{R}_k \boldsymbol{K}_k^T \end{cases} \tag{10}$$

where $\boldsymbol{K}$ is Kalman gain matrix; $\boldsymbol{R}$ is noise matrix of observations. As the navigation error state serves as the filter state, at last we feed back the estimated error state to the navigation state and reset the estimated error state to zero.

C. Pedestrian Motion Constraint

Pedestrian movement patterns characteristic in elevator and escalator scenarios are induced in Section II. Different movement patterns correspond to specific pedestrian motion constraint equations.

1) Elevator scenarios

According to the analysis of the elevator scenario in Section II, there is a brief static state before the elevator commences and after it concludes. ZUPT can be utilized to mitigate the accumulation of velocity errors. The velocity measurement equation can be written as

$$\delta \boldsymbol{z}_v = \hat{\boldsymbol{v}}^n - \tilde{\boldsymbol{v}}^n = \hat{\boldsymbol{v}}^n - [\,0 \;\; 0 \;\; 0\,]^T$$
$$\approx \delta \boldsymbol{v}^n + \boldsymbol{n}_v \tag{11}$$

where $\hat{\boldsymbol{v}}^n$ is the velocity estimated by INS; $\boldsymbol{n}_v$ is the noise of the velocity observations. Meanwhile, Zero Integrated Heading Rate (ZIHR) can also be applied to restrain the accumulation of heading errors[44]. The heading measurement equation can be written as

$$\delta \boldsymbol{z}_\psi = \hat{\psi} - \tilde{\psi} \approx \left[\frac{\partial \hat{\psi}}{\partial \boldsymbol{\phi}_x} \;\; \frac{\partial \hat{\psi}}{\partial \boldsymbol{\phi}_y} \;\; -1 \right] \boldsymbol{\phi} + \boldsymbol{n}_\phi$$

$$\frac{\partial \hat{\psi}}{\partial \boldsymbol{\phi}_x} = \frac{\boldsymbol{C}_{b,11}^n \cdot \boldsymbol{C}_{b,31}^n}{\boldsymbol{C}_{b,11}^n \cdot \boldsymbol{C}_{b,11}^n + \boldsymbol{C}_{b,21}^n \cdot \boldsymbol{C}_{b,21}^n} \tag{12}$$

$$\frac{\partial \hat{\psi}}{\partial \boldsymbol{\phi}_y} = \frac{\boldsymbol{C}_{b,21}^n \cdot \boldsymbol{C}_{b,31}^n}{\boldsymbol{C}_{b,11}^n \cdot \boldsymbol{C}_{b,11}^n + \boldsymbol{C}_{b,21}^n \cdot \boldsymbol{C}_{b,21}^n}$$

where $\hat{\psi}$ is the heading estimated by INS; $\tilde{\psi}$ is the heading at the first epoch when a pedestrian is in a stationary state; $\boldsymbol{C}_{b,ij}^n$ is the element in the i row and j column of the direction cosine matrix; n_ϕ is the noise of the heading observation.

In the multi-floor transit operation mode, the elevator is in a state of uniform motion, during which time acceleration update can be used to mitigate the spread of horizontal angles (roll and pitch). According to the formula (2), the acceleration measurement equation can be formulated as

$$\delta \boldsymbol{z}_f = \hat{\boldsymbol{f}}^n - \boldsymbol{f}^n = \hat{\boldsymbol{C}}_b^n \hat{\boldsymbol{f}}^b - \boldsymbol{f}^n$$
$$= (\boldsymbol{I} - \boldsymbol{\phi} \times) \boldsymbol{C}_b^n (\boldsymbol{f}^b + \boldsymbol{b}_f + \boldsymbol{n}_f) - \boldsymbol{f}^n \tag{13}$$
$$\approx \left[\left(\hat{\boldsymbol{C}}_b^n \hat{\boldsymbol{f}}^b \right) \times \right] \boldsymbol{\phi} + \hat{\boldsymbol{C}}_b^n \boldsymbol{b}_f + \hat{\boldsymbol{C}}_b^n \boldsymbol{n}_f$$

where $\hat{\boldsymbol{f}}^b$ is the output of accelerometer; $\hat{\boldsymbol{C}}_b^n$ is the direction cosine matrix estimated by INS; g is the local gravity acceleration; $\boldsymbol{b}_f$ is the bias of accelerometer; $\boldsymbol{n}_f$ is the noise of acceleration observations.

2) Escalator scenarios

Based on the analysis of the escalator scene in Section II, before ascending and after descending the escalator, NHC can be used to mitigate the divergence of velocity error[41]. According to the formula (3), the velocity measurement equation can be formulated as

$$\delta \boldsymbol{z}_v = \hat{\boldsymbol{v}}^b - \tilde{\boldsymbol{v}}^b = \hat{\boldsymbol{C}}_n^b \hat{\boldsymbol{v}}^n - (\boldsymbol{v}^b + \boldsymbol{n}_v)$$
$$= (\boldsymbol{I} - \boldsymbol{\phi} \times) \boldsymbol{C}_n^b (\boldsymbol{v}^n + \delta \boldsymbol{v}^n) - (\boldsymbol{v}^b + \boldsymbol{n}_v)$$
$$= \boldsymbol{C}_n^b \boldsymbol{v}^n + \boldsymbol{C}_n^b \delta \boldsymbol{v}^n - \boldsymbol{C}_n^b (\boldsymbol{v}^n \times) \boldsymbol{\phi} - \boldsymbol{v}^b - \boldsymbol{n}_v \tag{14}$$
$$\approx \hat{\boldsymbol{C}}_n^b \delta \boldsymbol{v}^n - \hat{\boldsymbol{C}}_n^b (\hat{\boldsymbol{v}}^n \times) \boldsymbol{\phi} - \boldsymbol{n}_v$$

where the direction cosine matrix $\hat{\boldsymbol{C}}_n^b$ denote the rotation of the n-frame with respect to the b-frame; $\hat{\boldsymbol{v}}^n$ is the velocity in n-frame estimated by INS. As pedestrians taking in the escalator, the lateral velocity is zero. Lateral ZUPT can be used in this case. The velocity measurement equation can be formulated from (14), it can be written as

$$\delta z_{v,lateral} = \delta \boldsymbol{z}_v [2] \tag{15}$$

where $\delta \boldsymbol{z}_v [2]$ is the element in the 2 rows of the (14). And as the escalator is in a state of uniform motion, acceleration update can also be used to mitigate the spread of horizontal angles, as formulated in equation (13).

3) Plane scenarios

In the plane scenarios, it can be assumed that the height change of the pedestrian is zero. Elevation locking can be used to constrain height drift. The position measurement equation can be formulated as

$$\delta \boldsymbol{z}_p = \hat{\boldsymbol{p}}^n - \tilde{\boldsymbol{p}}^n = \hat{\boldsymbol{p}}^n - [\,p_N \;\; p_E \;\; h_0\,]^T$$
$$\approx \delta \boldsymbol{p}^n + \boldsymbol{n}_p \tag{16}$$

where $\hat{\boldsymbol{p}}^n$ is the position estimated by INS; p_N and p_E are the plane position of pedestrian; h_0 is the constant height, generally measured after taking elevators or escalators; $\boldsymbol{n}_p$ is the noise of the position observations. Please note that we only need to use the third line (i.e. the height dimension) of this observation equation.

D. Reverse Smoothing

In the real-time location stage, measurements from the present and previous moments are used to estimate the current state. However, for non-real time location, subsequent measurements can also be utilized to optimize the current state. The reverse smoothing algorithm leverages measurements from the previous, present and following moments to estimate the current system state.

Once the pedestrian has traversed the elevator and escalator, the floor can be determined. All measurements while the pedestrian take in the elevator or escalator can be exploited to estimate height. Therefore, the reverse smoothing algorithm can be utilized in the system.

In this paper，RTS algorithm is applied to enhance height

estimation performance[42]. It can be formulated as

$$
\begin{cases}
\boldsymbol{K}_k = \boldsymbol{P}_{k,k}\boldsymbol{\Phi}_{k+1/k}^T\boldsymbol{P}_{k+1,k}^{-1} \\
\delta\hat{\boldsymbol{x}}_{k,N} = \delta\hat{\boldsymbol{x}}_{k,k} + \boldsymbol{K}_k(\delta\hat{\boldsymbol{x}}_{k+1,N} - \delta\hat{\boldsymbol{x}}_{k+1,k}) \\
\boldsymbol{P}_{k,N} = \boldsymbol{P}_{k,k} + \boldsymbol{K}_k(\boldsymbol{P}_{k+1,N} - \boldsymbol{P}_{k+1,k})\boldsymbol{K}_k^T \\
(k = N-1, N-2, ..., 0)
\end{cases} \quad (17)
$$

where $\boldsymbol{K}$ is the smoothing gain matrix; N is the total number of observations.

V. Experiments and Results

In this section, experiments have been designed to validate the feasibility of the algorithm proposed in Section III, which includes height estimation in both elevator and escalator scenarios. Additionally, several groups of 3D Pedestrian Dead Reckoning (PDR) cases are designed to demonstrate the effectiveness of the floor identification algorithms in 3D pedestrian navigation. Correspondingly, results for height estimation and PDR trajectories will also be presented.

A. Experimental Setting

Tests were conducted in multi-story buildings, with smartphones held steadily and at a specific angle during data collection, as shown in Fig. 4 and Fig. 5. There smartphones (i.e., HUAWEI Mate 40 Pro, Xiaomi 11, and Samsung Galaxy S20) were used for data collection. All sensors (gyroscope, accelerometer and magnetometer) have a data sampling rate of 50 Hz. The error model parameters of the IMU sensors are provided in Table I. Based on these parameters, the system's covariance matrix $\mathbf{q}(t)$ can be calculated, and the corresponding equivalent discretized covariance matrix $\boldsymbol{Q}$ can be obtained after discretization.

TABLE I
ERROR MODEL PARAMETERS OF THE IMU SENSORS

Parameter	Symbol	Value
Velocity random walk	VRW	$0.3\ m/s/\sqrt{h}$
Angle random walk	ARW	$0.3\ deg/\sqrt{h}$
STD of gyroscope bias	σ_{gb}	$0.03\ deg/s$
STD of accelerometer bias	σ_{ab}	$0.01\ m/s^2$
Correlation Time of accelerometer bias	T_{gb}	$4\ h$
Correlation Time of gyroscope bias	T_{ab}	$4\ h$

Fig. 4. Participant holding a smartphone in the elevator test.

Fig. 5. Participant holding a smartphone in the escalator test.

Meanwhile, to evaluate the accuracy of the proposed algorithm, we recorded atmosphere pressure data by barometer and calculated the corresponding heights for comparison. Two methods were employed for barometric altitude measurement: one based on the barometric pressure-to-height conversion formula[3], and the other using the Extended Kalman Filter (EKF) to integrate barometer data with inertial sensor data[45]. Additionally, we replicated an existing height estimation method based on inertial sensors, as describe in [33], for comparative purposes. This method

requires prior information about elevator and escalator speeds and escalator inclinations. The speeds and inclinations used in this method are shown in Table II. The method will be referred to as 'IMU' in the subsequent text.

TABLE II
PARAMETERS OF ELEVATORS AND ESCALATORS USED IN THE COMPARISON PLAN

Scenario	Parameter
Elevator	Speed: 2 m/s
Escalator	Speed: 0.5 m/s Inclination angle: 30 degrees

The data collection process for the experiments is outlined as follows:

1) Elevator

Participants held the smartphones and initiated the data collection software once they were stable after entering the elevator. They rode the elevator to a designated floor and stopped the software when the elevator halted and the doors fully opened.

2) Escalator

Participants approached the escalator, started data collection before stepping on, ascend to the next floor, and walked a short distance before stopping the software.

3) 3D PDR cases

Participants move freely in a shopping mall while holding the smartphones, including movements involving floor changes via elevators or escalators.

In elevator scenarios, pedestrians often traverse more than one or two floors, necessitating high accuracy in height estimation. Conversely, escalators typically span only one or two levels, so accurately identifying the direction of movement suffices for floor positioning needs.

B. Elevator Results

The testing scenario for the elevator experiment is a 17-story office building. The experiment involves taking the elevator up and down between 1st floor and 17th floor with intermediate stops, which simulates the real situation of pedestrians taking elevators in the multi-floor transit mode. The reference floor heights were measured by a laser range-finder.

Two observation corrections are employed in the elevator scenarios, one is the ZUPT and the other is the acceleration update. In this paper, the velocity standard deviation for the ZUPT is 0.02 m/s, and for the acceleration update, the acceleration standard deviation is 2.0 m/s² .

Figure. 6 and Figure. 7 depict two sets of the pedestrian height estimation results for taking the elevator up and down between the 1st floor and the 17th floor with intermediate stops.
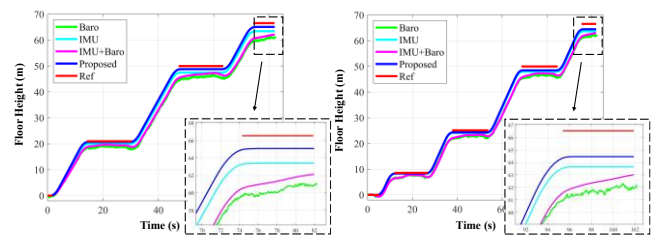

Fig. 6. Two sets of height estimation results from the 1st floor to the 17th floor by elevator.
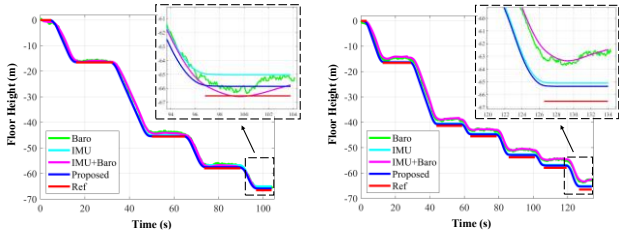
Fig. 7. Two sets of height estimation results from the 17th floor to the 1st floor by elevator.

Table III and Table IV present statistical summaries of height estimation error results between the 1st floor and the 17th floor with intermediate stops by taking the elevator. The error of the height estimation calculation formula is defined as:

$$Error = \frac{|\tilde{h} - \hat{h}|}{\tilde{h}} \times 100\% \tag{18}$$

where is $\tilde{h}$ the real height of the current floor; $\hat{h}$ is the estimated height of the current floor. Due to the inherent nature of inertial navigation systems as relative positioning tools that accumulate errors over time, we employ this relative error as a metric. As error divergence increases with duration, absolute error fails to serve as the optimal assessment criterion. Consequently, relative error provides a more accurate reflection of the solution's precision.

TABLE III
STATISTICAL SUMMARIES OF HEIGHT ESTIMATION ERROR FROM 1ST TO 17TH BY TAKING ELEVATORS

	Floor	Proposed	IMU	Baro	IMU + Baro
Elevator Up case 1	6	1.33%	4.81%	10.96%	9.39%
	13	2.38%	5.00%	8.24%	7.52%
	17	2.18%	4.72%	8.25%	8.48%
Elevator Up case 2	3	2.92%	2.92%	13.30%	8.28%
	7	3.34%	3.90%	12.30%	10.87%
	13	3.02%	4.08%	8.08%	7.54%
	17	3.11%	4.34%	7.23%	7.18%
Elevator Up case 3	3	4.32%	4.32%	10.04%	8.28%
	6	4.43%	4.05%	5.58%	5.82%
	13	3.24%	2.88%	6.38%	5.22%
	17	2.55%	3.02%	5.56%	4.57%
Error Mean		2.98%	4.00%	8.72%	7.56%

TABLE IV
STATISTICAL SUMMARIES OF HEIGHT ESTIMATION ERROR FROM 17TH TO 1ST BY TAKING ELEVATORS

	Floor	Proposed	IMU	Baro	IMU + Baro
Elevator Down case 1	13	0.48%	0.72%	4.10%	3.14%
	6	0.22%	1.19%	3.60%	3.49%
	3	0.69%	2.14%	1.85%	2.47%
	1	1.01%	2.27%	2.42%	1.91%
Elevator Down case 2	13	1.57%	1.81%	11.83%	11.23%
	7	1.59%	2.22%	7.87%	4.71%
	6	1.71%	2.28%	7.95%	5.42%
	4	1.69%	2.17%	7.21%	4.85%
	3	1.55%	2.00%	7.28%	4.99%
	1	1.77%	2.16%	6.72%	4.88%
Elevator Down case 3	13	1.21%	2.72%	5.07%	3.08%
	6	1.93%	1.36%	6.15%	4.50%
	3	2.31%	1.69%	6.85%	3.97%
	1	2.58%	2.04%	6.01%	4.13%
Error Mean		1.45%	1.91%	6.07%	4.48%

From the results, compare the error statistics of height estimation between the algorithm proposed in this paper and barometric altitude measurement for elevator scenarios, it's observed that the algorithm proposed in this paper offers better height estimation accuracy compared to the two methods of altitude measurement by barometer. Meanwhile, the height estimation method based on the barometer is easily affected by the surrounding environment. At the moment when the elevator doors open and close, the air

pressure inside the elevator is unstable due to the influence of air flow. Therefore, we conducted an additional set of height estimation experiment, as shown in Figure. 8. From the figure, it's observed that the height estimation result based on the barometric altitude formula is unstable due to air pressure fluctuations at the moment the doors open and close. On the contrary, the method proposed in this paper is not affected by the surrounding air pressure and temperature, resulting in higher stability.
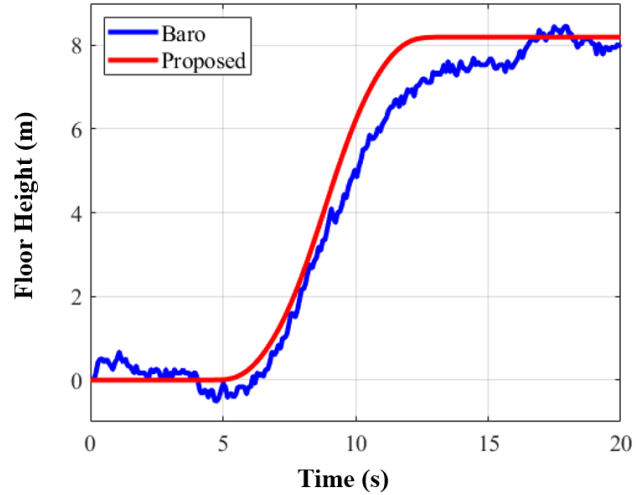

Fig. 8. Height estimation results from the 1st floor to the 6th floor by elevator.

Moreover, compared with the existing method based on IMU, the algorithm proposed in this paper exhibits slightly superior accuracy. Furthermore, the algorithm proposed in this paper does not require prior knowledge of the elevator's uniform speed, making it more universally applicable. In summary, the height estimation algorithm proposed in this paper can effectively meet the pedestrian floor identification needs in the elevator scenario.

C. Escalator Results

The escalator experiment was conducted in a shopping mall, involving traveling up and down between 1st floor and 2nd floor. The reference floor heights were also measured by a laser range-finder.

Three observation corrections are utilized in the escalator scenarios, one is the NHC, another is the lateral ZUPT, and the other is the acceleration update. The NHC correction primarily employs the constraint that the vertical velocity is zero, with a corresponding velocity standard deviation of 0.3 m/s. The velocity standard deviation for the lateral ZUPT is 0.05 m/s, and for the acceleration update, the acceleration standard deviation is 2.0 m/s² .

Figure. 9 and Figure. 10 illustrate two sets of the pedestrian height estimation results for the escalator experiment, depicting the height estimation while traveling up and down between the 1st floor and the 2nd floor.
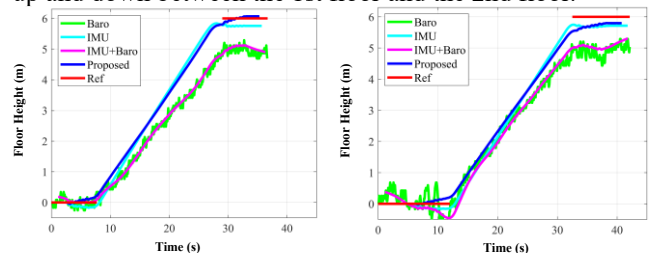
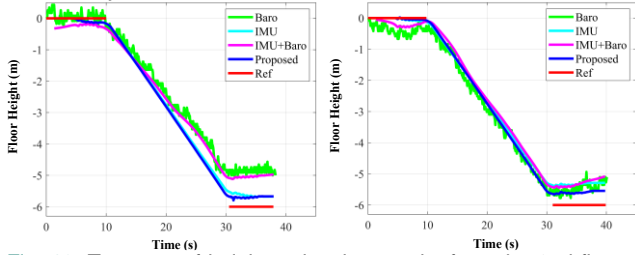Fig. 9. Two sets of height estimation results from the 1st floor to the 2nd floor by escalator.

Fig. 10. Two sets of height estimation results from the 2nd floor to the 1st floor by escalator.

Tabel V and Table VI present the statistical summaries of height estimation error results between the 1st floor and the 2nd floor by taking escalator. The error calculation method follows the formulation provided in equation (18).

TABLE V
STATISTICAL SUMMARIES OF HEIGHT ESTIMATION ERROR FROM 1ST TO 2ND BY TAKING ESCALATOR

Case	Proposed	IMU	Baro	IMU + Baro
1	1.17%	4.00%	19.17%	18.33%
2	3.33%	4.67%	20.50%	18.50%
3	2.83%	0.33%	21.67%	20.83%
4	3.83%	10.00%	20.33%	18.00%
5	4.33%	8.50%	24.67%	20.83%
6	5.50%	3.00%	22.00%	19.83%
Mean	**3.50%**	**5.08%**	**21.39%**	**19.39%**

TABLE VI
STATISTICAL SUMMARIES OF HEIGHT ESTIMATION ERROR FROM 2ND TO 1ST BY TAKING ESCALATOR

Case	Proposed	IMU	Baro	IMU + Baro
1	5.50%	5.50%	20.50%	17.50%
2	7.50%	11.83%	10.67%	10.83%
3	6.33%	0.50%	23.33%	21.50%
4	10.83%	12.67%	19.17%	16.83%
5	7.83%	11.17%	17.67%	14.67%
6	9.83%	6.00%	16.33%	15.67%
Mean	**7.97%**	**7.95%**	**17.95%**	**16.17%**

The results indicate a marginally higher accuracy in height estimation when pedestrians take the escalator up compared to downward. This phenomenon aligns with findings from existing methods based on IMU. This discrepancy can be attributed to the dynamic of pedestrian motion, where a slight upward vertical velocity occurs as pedestrians step onto the escalator. During upward escalator movement, this vertical motion aligns with the escalator's vertical velocity, whereas during downward movement, it is nearly opposite. Consequently, the accuracy of height estimation is marginally compromised when pedestrians take the escalator downward.

To provide a robust comparison, we conducted statistical analyses between the proposed method and other methods shown in the tables. Across both tables, the proposed method consistently shows lower error percentages compared to the Baro Methods. Additionally, as shown in Fig. 9 and Fig. 10, similar to the elevator scenario, the pressure instability caused by pedestrian movement can lead to unstable height estimation. In contrast, the method proposed in this paper, based solely on IMU, is not affected by the surround environment, thereby ensuring higher stability.

In summary, the method proposed in this paper offers notable advantages over existing methods based on IMU. It maintains notable accuracy in height estimation without the need for prior information. Moreover, it demonstrates a significant improvement in accuracy compared to the two methods of height estimation by barometer. Consequently, the height estimation method for escalator scenarios effectively meets the requirements for pedestrian floor identification.

D. Reverse smoothing algorithm

The RTS indeed provides stable results by incorporating previous, present, and future measurements. However, the reverse smoothing algorithm does not affect the final navigation (height estimation) result. Its primary purpose is to make the trajectory smoother and more consistent with the actual path. Figure. 11 and Figure. 12 compare the proposed method with and without RTS in elevator and escalator scenarios, demonstrating the effectiveness of RTS.
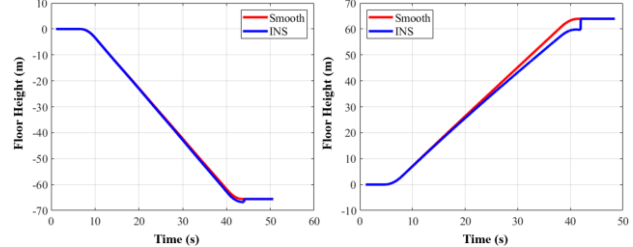

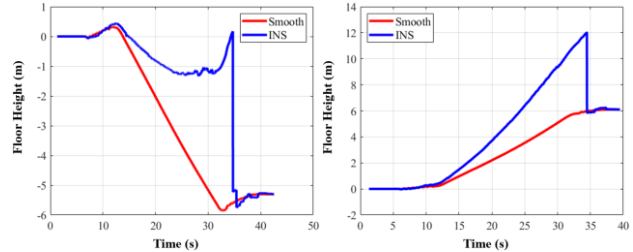Fig. 11. Comparison of Height Estimation with and without RTS in Elevator Scenarios.

Fig. 12. Comparison of Height Estimation with and Without RTS in Escalator Scenarios

For pedestrians who need to determine which floor they are on, knowing their current height in real-time is unnecessary. They only need to calculate their height upon reaching a specified floor to determine their location. Therefore, RTS is not absolutely essential in the algorithm proposed in this paper. Its role is merely to reflect the true trend of the user's height changes.

E. 3D PDR Case Study

The experiment for the 3D PDR case was conducted in a multi-story shopping mall. Participants were instructed to walk freely throughout the various floors of the building, transitioning between levels via elevators and escalators. The reference truth of floor heights were provided by a laser range-finder. Meanwhile, in this paper we focus on the pedestrian height estimation. The precision of horizontal positioning offered by PDR is not the focal point of our interest. Consequently, in the process of deriving the 3D PDR solution, the approach involves overlaying the height information estimated by the method proposed in this paper onto the respective horizontal positions calculated by PDR.

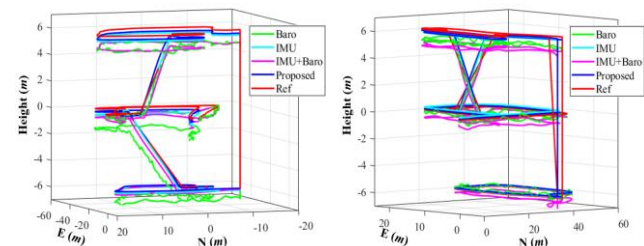Figure. 13 depicts the trajectories of the two cases of the 3D PDR.

Fig. 13. The Trajectories of the pedestrian estimated by PDR and estimation algorithm.

Figure. 14 shows the height estimation results of the estimated results and the reference truth.
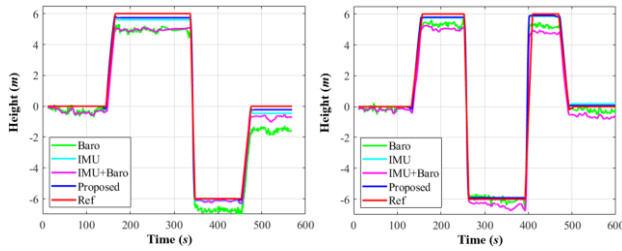

Fig. 14. Height estimation result calculated by the proposed height estimation algorithm.

The result illustrated in both the trajectory plot and height estimation plot clearly demonstrate the effectiveness of the floor identification method proposed in this paper. This method precisely estimates the height of pedestrians after they transition between floors via elevators and escalators, facilitating accurate determination of the current floor level. Unlike traditional PDR methods that lack the capability to discern floor levels, the method proposed in this paper offers a viable and practical solution for pedestrian floor identification, addressing a significant gap in indoor navigation systems.

VI. Conclusion and Future Work

In this paper, a pedestrian floor identification method based on inertial sensors in smartphones is proposed. By investigating the unique motion characteristics of pedestrians in elevator and escalator scenarios, we designed appropriate motion constraint models corresponding to these contexts. The core algorithmic framework is based on INS, employing the EKF to integrate pedestrian motion constraint, thus estimating the height changes as pedestrians transition between floors. The precision of height estimation achieved by the proposed method outperforms current IMU-based and barometer-based methods, exhibiting relative errors in elevator scenarios of 2.98% during upward and 1.45% during downward. In escalator scenarios, the method demonstrates relative errors of 3.50% for upward and 7.97% for downward movements. Moreover, the method proposed in this paper offers a promising solution for height estimation in the case study of 3D PDR.

The floor identification methods proposed in this paper address the essential positioning requirements for pedestrian users, exhibiting high reliability, extensive scalability, and cost-effectiveness. However, there are several limitations that need to be addressed. One of the primary challenges is the precise determination of the pedestrian's movement scenario. The current method relies on manual calibration for scenario recognition, and future research should focus on developing robust algorithms for automatic scenario recognition. Another challenge is the adaptation to various holding modes. The method in this paper only considers the horizontal holding mode of smartphones. However, in daily use, people hold their smartphones in various ways. Future research could explore how different holding modes affect the accuracy of height estimation.

Reference

[1] I. A. Junglas and R. T. Watson, "Location-based services," Commun. ACM, vol. 51, no. 3, pp. 65–69, Mar. 2008, doi: 10.1145/1325555.1325568.

[2] M. F. Mokbel and J. J. Levandoski, "Toward context and preference-aware location-based services," in Proceedings of the Eighth ACM International Workshop on Data Engineering for Wireless and Mobile Access, in MobiDE '09. New York, NY, USA: Association for Computing Machinery, Jun. 2009, pp. 25–32. doi: 10.1145/1594139.1594150.

[3] B. Li, H. Bruce, and G. Thomas, "Using barometers to determine the height for indoor positioning," presented at the International Conference on Indoor Positioning and Indoor Navigation, Montbeliard-Belfort: IEEE, 2013, pp. 1–7.

[4] Q. Wang et al., "Recent advances in floor positioning based on smartphone," Measurement, vol. 214, p. 112813, Jun. 2023, doi: 10.1016/j.measurement.2023.112813.

[5] H. Rizk, M. Torki, and M. Youssef, "CellinDeep: Robust and Accurate Cellular-based Indoor Localization via Deep Learning," IEEE Sensors Journal, vol. 19, no. 6, pp. 2305–2312, 2018.

[6] F. Gu, B. Jorg, K. Kourosh, G. Jan, and V. Shahrokh, "ZeeFi: Zero-effort floor identification with deep learning for indoor localization," presented at the 2019 IEEE Global Communications Conference (GLOBECOM), Waikoloa, HI, USA, 2019, pp. 1–6.

[7] S. Głowiński, A. Błażejewski, T. Królikowski, and R. Knitter, "Gait Recognition: A Challenging Task for MEMS Signal Identification," in Sustainable Design and Manufacturing 2019, P. Ball, L. Huaccho Huatuco, R. J. Howlett, and R. Setchi, Eds., Singapore: Springer, 2019, pp. 473–483. doi: 10.1007/978-981-13-9271-9_39.

[8] P. Bhargava, S. Krishnamoorthy, A. K. Nakshathri, M. Mah, and A. Agrawala, "Locus: An Indoor Localization, Tracking and Navigation System for Multi-story Buildings Using Heuristics Derived from Wi-Fi Signal Strength," in Mobile and Ubiquitous Systems: Computing, Networking, and Services, K. Zheng, M. Li, and H. Jiang, Eds., in Lecture Notes of the Institute for Computer Sciences, Social Informatics and Telecommunications Engineering. Berlin, Heidelberg: Springer, 2013, pp. 212–223. doi: 10.1007/978-3-642-40238-8_18.

[9] L. Xu, "A K-Means Based Method to Identify Floor in WLAN Indoor Positioning System," IEEE Software, 2012, Accessed: Mar. 05, 2024. [Online]. Available: https://www.semanticscholar.org/paper/A-K-Means-Based-Method-to-Identify-Floor-in-WLAN-Xu/662f0b41eb732918ca616b0ada0eefd60a6cd750#citing-papers

[10] J. Luo, Z. Zhang, C. Wang, C. Liu, and D. Xiao, "Indoor Multifloor Localization Method Based on WiFi Fingerprints and LDA," IEEE Transactions on Industrial Informatics, vol. 15, no. 9, pp. 5225–5234, Sep. 2019, doi: 10.1109/TII.2019.2912055.

[11] L. Sun, Z. Zheng, T. He, and F. Li, "Multifloor Wi-Fi Localization System with Floor Identification," International Journal of Distributed Sensor Networks, vol. 11, no. 7, p. 131523, Jul. 2015, doi: 10.1155/2015/131523.

[12] K. S. Hosseini, M. H. Azaddel, M. A. Nourian, and A. A. Azirani, "Improving Multi-floor WiFi-based Indoor positioning systems by Fingerprint grouping," in 2021 5th International Conference on Internet of Things and Applications (IoT), May 2021, pp. 1–6. doi: 10.1109/IoT52625.2021.9469602.

[13] A. Varshavsky, A. LaMarca, J. Hightower, and E. de Lara, "The SkyLoc Floor Localization System," presented at the Fifth Annual IEEE International Conference on Pervasive Computing and Communications (PerCom'07), White Plains, NY, USA: IEEE, 2007, pp. 125–134.

[14] M. A. A. Rahman, M. Dashti, and J. Zhang, "Floor determination for positioning in multi-story building," presented at the 2014 IEEE Wireless Communications and Networking Conference (WCNC), Istanbul, Turkey: IEEE, 2014, pp. 2540–2545.

[15] Z. Zheng, Y. Chen, S. Chen, L. Sun, and D. Chen, "Bigloc: a two-stage positioning method for large indoor space," International Journal of Distributed Sensor Networks, vol. 12, no. 6, p. 1289013, 2016.

[16] A. Saeed, A. Wasfey, H. Rizk, and H. Yamaguchi, "CellStory: Extendable cellular signals-based floor estimator using deep learning," presented at the 2022 18th International Conference on Intelligent Environments (IE), Biarritz, France: IEEE, 2022, pp. 1–4.

[17] R. Elbakly, H. Aly, and M. Youssef, "TrueStory: Accurate and robust RF-based floor estimation for challenging indoor environments," IEEE Sensors Journal, vol. 18, no. 24, pp. 10115–10124, 2018.

[18] R. Elbakly and M. Youssef, "The StoryTeller: Scalable building-and ap-independent deep learning-based floor prediction," Proceedings of the ACM on Interactive, Mobile, Wearable and Ubiquitous Technologies, vol. 4, no. 1, pp. 1–20, 2020.

[19] K. Alkiek, A. Othman, H. Rizk, and M. Youssef, "Deep Learning-based Floor Prediction Using Cell Network Information," presented at the Proceedings of the 28th International Conference on Advances in Geographic Information Systems, 2020, pp. 663–664.

[20] H. Rizk, H. Yamaguchi, T. Higashino, and M. Youssef, "A ubiquitous and accurate floor estimation system using deep representational learning," presented at the Proceedings of the 28th International Conference on Advances in Geographic Information Systems, 2020, pp. 540–549.

[21] H. Ye, T. Gu, X. Tao, and J. Lu, "F-Loc: Floor localization via crowdsourcing," presented at the 2014 20th IEEE international conference on parallel and distributed systems (ICPADS), IEEE, 2014, pp. 47–54.

[22] X. Shen, Y. Chen, J. Zhang, L. Wang, G. Dai, and T. He, "BarFi: Barometer-aided Wi-Fi floor localization using crowdsourcing," presented at the 2015 IEEE 12th International Conference on Mobile Ad Hoc and Sensor Systems, Dallas, TX, USA: IEEE, 2015, pp. 416–424.

[23] R. Elbakly, M. Elhamshary, and M. Youssef, "HyRise: A robust and ubiquitous multi-sensor fusion-based floor localization system," Proceedings of the ACM on interactive, mobile, wearable and ubiquitous technologies, vol. 2, no. 3, pp. 1–23, 2018.

[24] Y. Shu, C. Bo, G. Shen, C. Zhao, L. Li, and F. Zhao, "Magicol: Indoor Localization Using Pervasive Magnetic Field and Opportunistic WiFi Sensing," IEEE J. Select. Areas Commun., vol. 33, no. 7, pp. 1443–1457, Jul. 2015, doi: 10.1109/JSAC.2015.2430274.

[25] M. Zhao, D. Qin, R. Guo, and X. Wang, "Indoor Floor Localization Based on Multi-Intelligent Sensors," ISPRS International Journal of Geo-Information, vol. 10, no. 1, Art. no. 1, Jan. 2021, doi: 10.3390/ijgi10010006.

[26] I. Ashraf, S. Hur, M. Shafiq, and Y. Park, "Floor Identification Using Magnetic Field Data with Smartphone Sensors," Sensors, vol. 19, no. 11, Art. no. 11, Jan. 2019, doi: 10.3390/s19112538.

[27] M. Yu, F. Xue, C. Ruan, and H. Guo, "Floor positioning method indoors with smartphone's barometer," Geo-Spatial Information Science, vol. 22, no. 2, pp. 138–148, 2019.

[28] H. Ye, T. Gu, X. Tao, and J. Lu, "Scalable floor localization using barometer on smartphone," Wireless Communications and Mobile Computing, vol. 16, no. 16, pp. 2557–2571, 2016.

[29] B. Shin et al., "Motion recognition-based 3D pedestrian navigation system using smartphone," IEEE Sensors Journal, vol. 16, no. 18, pp. 6977–6989, 2016.

[30] H. Zhao, W. Cheng, N. Yang, S. Qiu, Z. Wang, and J. Wang, "Smartphone-based 3D indoor pedestrian positioning through multi-modal data fusion," Sensors, vol. 19, no. 20, p. 4554, 2019.

[31] H. Xia, X. Wang, Y. Qiao, J. Jian, and Y. Chang, "Using Multiple Barometers to Detect the Floor Location of Smart Phones with Built-in Barometric Sensors for Indoor Positioning," Sensors, vol. 15, no. 4, Art. no. 4, Apr. 2015, doi: 10.3390/s150407857.

[32] H. Ye et al., "FTrack: Infrastructure-free floor localization via mobile phone sensing," presented at the 2012 IEEE International Conference on Pervasive Computing and Communications, Lugano: IEEE, 2012, pp. 2–10.

[33] X. Li et al., "A Pedestrian 3-D Position Estimation Method Based on Equality Constraint and Moving Platforms Correction Model," IEEE Sensors Journal, vol. 22, no. 20, pp. 19596–19607, 2022.

[34] O. Woodman and R. Harle, "Pedestrian localisation for indoor environments," in Proceedings of the 10th international conference on Ubiquitous computing, in UbiComp '08. New York, NY, USA: Association for Computing Machinery, Sep. 2008, pp. 114–123. doi: 10.1145/1409635.1409651.

[35] E. M. Diaz, S. Kaiser, and D. B. Ahmed, "Height error correction for shoe-mounted inertial sensors exploiting foot dynamics," Sensors, vol. 18, no. 3, p. 888, 2018.

[36] N. Bai, Y. Tian, Y. Liu, Z. Yuan, Z. Xiao, and J. Zhou, "A high-precision and low-cost IMU-based indoor pedestrian positioning technique," IEEE Sensors Journal, vol. 20, no. 12, pp. 6716–6726, 2020.

[37] J. Wang, X. Xu, Z. Yu, Z. Li, and S. Liu, "A Novel Suppression Method of Height Drift for Pedestrian Navigation With a Circular Hypotheses on Terrain Slope," IEEE Sensors Journal, vol. 22, no. 12, pp. 12054–12063, 2022.

[38] S. H. Shin, C. G. Park, J. W. Kim, H. S. Hong, and J. M. Lee, "Adaptive step length estimation algorithm using low-cost MEMS inertial sensors," presented at the 2007 IEEE sensors applications symposium, San Diego, CA, USA: IEEE, 2007, pp. 1–5.

[39] Y. Wang et al., "Spatial Structure-Related Sensory Landmarks Recognition Based on Long Short-Term Memory Algorithm," Micromachines, vol. 12, no. 7, Art. no. 7, Jul. 2021, doi: 10.3390/mi12070781.

[40] Z. Wang, H. Zhao, S. Qiu, and Q. Gao, "Stance-phase detection for ZUPT-aided foot-mounted pedestrian navigation system," EEE/ASME Transactions On Mechatronics, vol. 20, no. 6, pp. 3170–3181, 2015.

[41] X. Niu, S. Nassar, and N. El-Sheimy, "An Accurate Land-Vehicle MEMS IMU/GPS Navigation System Using 3D Auxiliary Velocity Updates," Navigation, vol. 54, no. 3, pp. 177–188, 2007.

[42] P. N. Raanes, "On the ensemble Rauch-Tung-Striebel smoother and its equivalence to the ensemble Kalman smoother," Quarterly Journal of the Royal Meteorological Society, vol. 142, no. 696, pp. 1259–1264, 2016.

[43] Q. Chen, X. Niu, Q. Zhang, and Y. Cheng, "Railway track irregularity measuring by GNSS/INS integration," Navigation: Journal of The Institute of Navigation, vol. 62, no. 1, pp. 83–93, 2015.

[44] W. Zhang, X. Li, D. Wei, X. Ji, and H. Yuan, "A foot-mounted pdr system based on imu/ekf+ hmm+ zupt+ zaru+ hdr+ compass algorithm," presented at the 2017 International conference on indoor positioning and indoor navigation (IPIN), Sapporo, Japan: IEEE, 2017, pp. 1–5.

[45] Z. Bang, Z. H. U. Jinxin, X. U. Zhengyi, L. I. U. Pan, and W. E. I. Jianming, "Bayesian network-based floor localization algorithm," Journal of Computer Applications, vol. 39, no. 8, p. 2468, Aug. 2019, doi: 10.11772/j.issn.1001-9081.2019010119.

Shiyi Chen received the B.Eng. degree in navigation engineering from Wuhan University, Wuhan, China, in 2023, where he is currently pursuing the master's degree in surveying and mapping engineering.

His research interests focus on inertial navigation, sensor fusion algorithm, pedestrian navigation, and indoor positioning.

Jian Kuang received the B.Eng. degree and Ph.D. degree in Geodesy and Survey Engineering from Wuhan University, Wuhan, China, in 2013 and 2019, respectively.

He is currently a Postdoctoral Fellow with the GNSS Research Center in Wuhan University, Wuhan, China. His research interests focus on inertial navigation, pedestrian navigation and indoor positioning.

Dazhou Xia received the B.Eng. degrees in navigation engineering from Wuhan University, Wuhan, China, in 2022, where he is currently pursuing the master's degree in geodesy and surveying engineering.

His research interests focus on inertial navigation, sensor fusion algorithms, pedestrian navigation, and indoor positioning.

Xiaoji Niu is a Professor at GNSS Research Center in Wuhan University, China. He got his Ph.D. and bachelor degrees (with honors) by the Department of Precision Instruments at Tsinghua University in 2002 and 1997, respectively.

He performed postdoctoral research at the University of Calgary, Canada, and worked as a senior scientist at SiRF Technology Inc. Dr. Niu is currently leading the Integrated & Intelligent Navigation (i2Nav) group. His research interests focus on GNSS/INS integration, low-cost navigation sensor fusion, and relevant new applications. Dr. Niu has published 200+ academic papers and owns 30+ patents.